Heat transfer of uncoated and nanostructure coated commercially micro-enhanced refrigeration tubes under pool boiling conditions

Dian Dickson[a], Bradley D. Bock[a]* and John R. Thome[b]

This is the POST PRINT version of this article. The final, published version of the article can be found at:
https://doi.org/10.1016/j.applthermaleng.2023.121757

[a]*Department of Mechanical and Aeronautical Engineering, Faculty of Engineering, the Built Environment and IT, University of Pretoria, Pretoria, South Africa*
[b]*JJ Cooling Innovation, Ecole Polytechnique Fédérale de Lausanne (EPFL) Park, Bâtiment A, CH-1015 Lausanne, Switzerland*

ABSTRACT

The heat transfer performance of commercially produced micro-enhanced tubes with and without a nanocoating was investigated under pool boiling of saturated refrigerant. These multiscale enhancements were on the outside of 19 mm horizontal copper tubes heated by water to determine the effectiveness of this multiscale enhancement technique on industrially relevant tubes and geometry. The tubes tested were a plain tube roughened by sandpaper, a low finned GEWA-KS tube and two micro-enhanced re-entrant cavity tubes, the GEWA-B5 and EHPII. The tubes were tested in R134a at saturation temperatures of 5°C and 25°C across a range of heat fluxes from 20 kW/m^2 to 100 kW/m^2 under pool boiling conditions. The nanocoating applied to the tubes produced a forest of copper oxide nanostructures on the surface, increasing wickability of the surface. A Scanning Electron Microscopy showed that copper oxide nanocoatings coated all micro-enhanced tubes evenly without impeding the surface features or significantly blocking the re-entrant cavities. For the uncoated tubes in pool boiling, the heat transfer coefficients of the EHPII was up to 519% greater than those of the plain roughened tube, the GEWA-B5 was up to 539% higher than the roughened tube and the GEWA-KS was at best 64% higher than those of the plain roughened tube. Increases in the saturation temperature to 25°C produced minor improvements in heat transfer coefficients. The application of the copper oxide nanocoating resulted in generally decreased heat transfer performance by approximately 40% on average compared to the uncoated tubes, with the GEWA-B5 tube the worst affected. Degradation of the heat transfer is thought on plain surfaces to be due to the flooding of nucleation sites, while re-entrant cavity style enhanced surfaces were thought to experience degraded sensible and latent heat transfer due to impeded flow in the microstructure capillary channel, as bubbles were noted to be trapped in the channels. It is recommended that the heat transfer at much higher heat flux ranges be explored for possible HTC enhancement.

Keywords: nanostructures; multiscale; heat transfer coefficients; pool boiling; 3D enhanced

* Corresponding author
Email address: bradley.bock@up.ac.za

Nomenclature

Symbol	
C	constant or coefficient
c_p	specific heat capacity $[J/kg \cdot K]$
D	diameter $[m]$
d	difference $[m]$
f	friction factor
pH	power of Hydrogen
h	heat transfer coefficient $[W/m^2 \cdot K]$
k	thermal conductivity $[W/m \cdot K]$

K	ratio
m	mass $[kg]$
Nu	Nusselt number
Pr	Prandtl number
q	heat flux $[W/m^2]$
R	thermal resistance $[m^2 \cdot K/W]$
Re	Reynolds number
T	temperature $[K]$
U	overall heat transfer coefficient $[W/m^2 \cdot K]$
x	length $[m]$

Subscripts

ave	average
CuO	copper oxide nanocoated
g	gas
Gnie	attributed to Gnielinski's correlation
h	hydraulic (effective Reynolds diameter)
i	with respect to tube inside
mid	midpoint of tube
o	with respect to tube outside
or	outer root diameter
q	with respect to heat flux
r	refrigerant
sat	saturated state
surf	relative to plain surface
sup	wall superheat
t	with respect to the tube wall
T	with respect to temperature
w	water

Abbreviations

CO_2	Carbon dioxide
CuO	Copper Oxide
enhanced	With respect to the 3D microstructured tube
Ra	Roughness Average
roughened	With respect to the plain roughened tube
CA	Contact Angle
CERG	Clean Energy Research Group
CHF	Critical Heat Flux
FF	Falling Film
fpi	fins per inch
fps	frames per second
HTC	Heat Transfer Coefficient
pH	Power of Hydrogen
PTFE	Polytetrafluoroethylene
Re	Reynolds number
RO	Reverse Osmosis
SEM	Scanning Electron Microscope
UP	University of Pretoria

1. Introduction

Pool boiling of refrigerants on the outside of tubes is a commercially important process, with applications in a wide array of fields, from current uses in fields such as refrigeration and nuclear energy, to future opportunities in electronics cooling and solar energy generation. Solar energy generation using refrigerants in organic Rankine cycles [1, 2] in particular still requires substantial improvements in heat transfer effectiveness to reduce capital costs to allow for competitiveness with existing photovoltaic systems [3].

Refrigeration tube manufacturers commercially produce many micro-enhanced tubes that enhanced the outside tube surface heat transfer coefficients (HTCs). The addition of fins primarily increases the heat transfer through increased surface area [4] while re-entrant cavities are used for pool boiling to increase heat transfer through the action of the fluid flowing through the cavity network driven by a bubble pumping action, resulting in increased sensible and evaporation heat transfer, while also increasing nucleation site density [5].

Multiscale enhancements however may offer the next step in heat transfer enhancement. It was observed that there was an impact on heat transfer by multiple surface enhancements through micro dendritic fin arrays on a copper substrate which increased HTCs by approximately 200% compared to a plain surface in a review by Liang and Mudawar [6]. Commercially micro-enhanced tubes comprise tubes with intricate 3D structures easily visible on its surface which preliminary enhances heat transfer. A multiscale enhancement approach is undertaken where these 3D enhanced tubes are coated with a nanostructure coating which may enhance the heat transfer coefficients even further in a quick and inexpensive way. A study by Im et al. [7] in the same review recorded an undisclosed but measurable improvement in HTCs under pool boiling conditions on a multiscale surface composed of microgrooves with CuO flower-like nanocoatings.

A variety of nanocoatings exist, typically with the focus of creating either hydrophobic or hydrophilic surface properties, as well as other relevant properties, such as surface wickability. Typically, on plain surfaces, it is believed that hydrophilic coatings deliver lower HTCs under pool boiling than hydrophobic coatings as they result in HTC degradation from nucleation site flooding [8-12].

An experimental study by Sen et al. [13] conducted water pool boiling heat transfer on copper oxide (CuO) nanocoated copper plate surfaces prepared with grade 1000 grit sandpaper to micro-enhance the tube for more nucleation sites. The creation of both hydrophilic and hydrophobic surfaces was possible through simple changes to the same base chemical solution used for the coating. It was found that the enhanced capillary action feeding water to the microstructure nucleation sites prohibited early onset of a vapour blanket to increase the CHF point. It was also found that the CuO nanocoated hydrophobic surface enhanced the heat transfer the most, with HTCs approximately 2 times more than the bare copper surface. The hydrophilic surface also enhanced heat transfer, where the HTCs were approximately 1.3 times more than the bare copper surface HTCs at best. It was stated that the hydrophobic surface requires less surface energy for the onset of nucleate boiling – where the low affinity to liquid by the surface influence the wettability to result in lower energy exertion by the surface tension of the liquid to draw up away from the surface. However, such surfaces reaches the CHF point very soon as opposed to the hydrophilic surface [13].

An experimental investigation by Patel et al. [14] tested boiling of water on CuO nanocoated copper plates showed that the hydrophilic surface increased HTCs between 40% and 80%. The CuO coating synthesis was through a spinning technique which increased the wettability and nucleation site density [14]. The roughness was also increased by this particular CuO coating type and is the likely cause of the significant increase in nucleation site density.

When considering multiscale enhancements, the interaction of the hydrophilic nanostructures together with microstructures may be beneficial, as studies [6, 15, 16] suggest high surface wettability from extreme hydrophilic nanocoatings may increase HTCs on micro-enhanced tubes under pool boiling due to less internal dryout among the microstructures during boiling because of the surface's strong liquid affinity. This has been proven for microstructures that themselves wick liquids. A study by Kunugi et al. [17] found HTC enhancement through a CuO nanoparticle coating performing around 200% better than a bare copper plate for a co-current heat exchanger case, as well as performing heat transfer experiments on CuO, carbon-nanotube and aluminium oxide coatings on plain copper to show an approximate 180% heat transfer enhancement. However, the exact mechanism for this heat transfer remains vague and requires further investigation. A significant observation was that the cases in which HTC enhancement took place was mostly on porous nanocoatings. It should be noted though that this can also be achieved with microporous coatings. Lee et al. [18] created porous layers as micro-scale enhancements by coating copper powders through a sintering process on plain tubes to enhance wettability and improve wicking. It was found that the heat transfer was doubled through the aid of the coating facilitating capillary wicking for complete wetting.

When using nanostructures to facilitate the wicking, the results appear to be unclear among literature regarding the enhancement of heat transfer. This can be observed as by the experiments where copper micropillars have been oxidized to create a 'structured' CuO nanocoating by Chu et al. [6, 10, 19]. Vertical copper dendrites in a multiscale enhancement fashion have also been used to create very intricate enhanced surfaces, which resulted in boiling HTCs as much as twice of the plain copper surface [6, 20].

Rahman and McCarthy [21] analysed the mechanisms of HTC enhancement by a variety of CuO nanocoated plain copper substrates. It was found that a hydrophilic CuO nanostructure coating degraded HTCs significantly by approximately 19% through restricting nucleation sites and was attributed to the smaller nucleation site activity requiring a greater superheat to activate them. A hydrophobic-hydrophilic surface constructed from

polytetrafluoroethylene (PTFE) dots on a hydrophilic substrate was found to increase nucleation activation and enhance heat transfer by 116% compared to the plain hydrophilic substrate. Another more complex design of a heterogeneous surface was intuitively constructed to combine the hydrophobic and hydrophilic properties by alternating between superhydrophobic PTFE and CuO coated strips on the surface to induce mixed wettability to enhance both HTCs and the CHF. The PTFE coatings were shown to lower the superheat required for nucleation and consequently enhanced HTCs, while the combination of PTFE and CuO on the heterogenous surface proved to greatly enhance the ebullition cycle through the hydrophilic portions of the surface where liquid wickability was desired and the hydrophobic portions of the surface where nucleation and heat transfer was desired. These biphilic surfaces outperformed normal nanocoated surface with a 270% increase in HTCs [21].

A case of heat transfer enhancement was observed by Xu and Li [22] where the HTCs were increased through a CuO nanocoated grooved plate by a maximum of 15%. They also tested an uncoated and a CuO nanocoated flat grooved plate. Their experiments indicated that heat transfer enhancement took place during tests where the flat plate was simultaneously heated and cooled at different regions along with continuous boiling. It was speculated that the heat transfer enhancement was due to the super-hydrophilic surface created by the CuO nanocoating, where the prevention of dryout was enforced by coolant being wicked to the dryout spots as opposed to the uncoated flat plate.

A chlorofluoro hydrophobic coating applied to commercially enhanced microstructured tubes under falling film boiling was compared to uncoated tubes in a study performed by Jin et al. [8] and showed an increase of up to 60% in HTCs. It was speculated that the hydrophobic coating offered less frictional resistance for two-phase flow through the micro capillary channels to aid in the liquid supply to nucleation sites and to assist in the bubble pumping action [8].

The majority of the studies on multiscale enhancements thus have focussed on adding nanostructures onto laboratory developed microstructures up to this point, typically using sintered porous structures, microchannels, fins and pin fins [6, 23, 24] or meshes [25]. Depending on the definition of multiscale enhancement, practically none use re-entrant microcavities [6, 25], and none to our knowledge combine the current industrially developed microstructures, the so-called 3D enhanced surfaces such as the Turbo-B or GEWA-B series of pool boiling surfaces, with nanostructures. Previous studies have typically also been conducted on small flat plates instead of the more industrially relevant tube geometry, and typically do not use pressurised HFC refrigerant, but rather water or fluorinerts at atmospheric pressure.

Thus there is an opportunity to test whether nanostructure induced surface wicking can beneficially combine with the network of re-entrant cavities present on 3D enhanced tubes under the industrially relevant conditions of pressurized refrigerant.

This study experimentally investigates the effect of multiscale enhancements on heat transfer of refrigerant pool boiling by coating commercially produced enhanced copper tubes with a wickable CuO nanocoating. This is done in the hope of combining the two sets of beneficial heat transfer mechanisms the two scales of enhancement have previously seen to provide. A plain, low finned and two '3D enhanced' re-entrant cavity style tubes will be tested at 5°C and 25°C in refrigerant R-134a across a heat flux range of 20 kW/m^2 to 100 kW/m^2 where the heating is provided by water. This study also provides an opportunity to publish pool boiling data for 19 fpi GEWA-KS and EHPII tubes with R-134a in the open academic literature for the first time.

2. Experimental setup

2.1. Experiment facility

The falling film (FF) boiling rig at the University of Pretoria (UP) was used to perform the pool boiling experiments. The detailed description of the FF rig can be found in Roques [26] and Bock [16], but the refrigerant circuit and test chamber shown in Figure 2-1 are briefly described here.

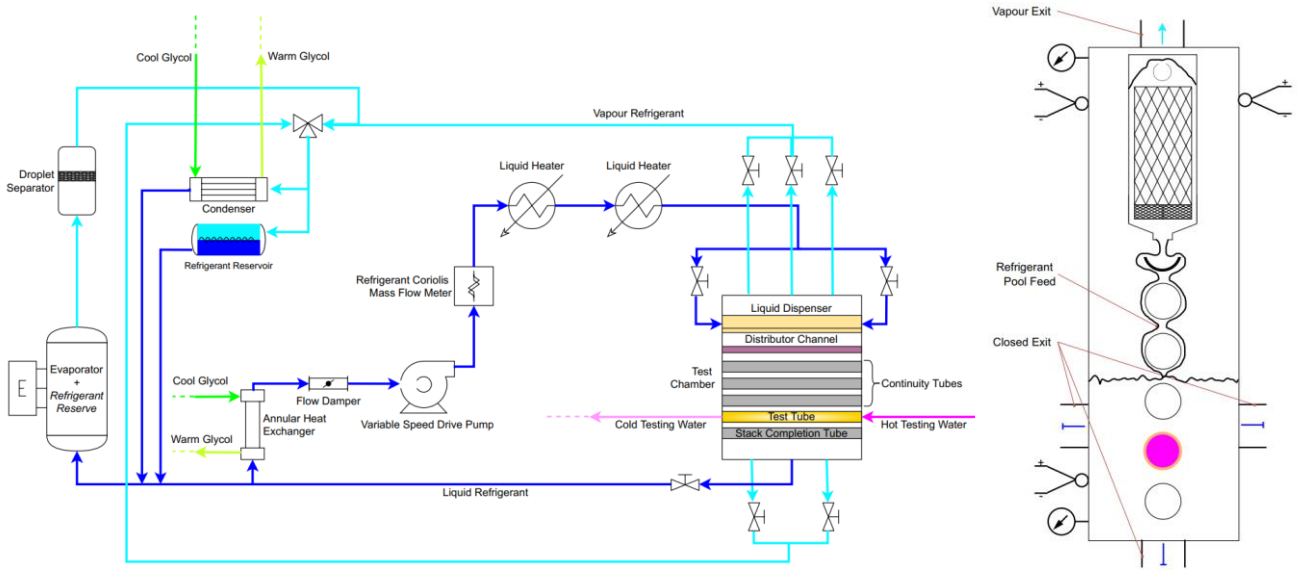

(a) Refrigerant circuit (b) Test chamber

Figure 2-1: Schematic of the refrigerant circuit including the test chamber in pool boiling configuration

The refrigerant circuit , shown in Figure 2-1 (a), conditions the refrigerant and controls the saturation pressure to the set point for a study through the combination of electrical kettle evaporator and an overhead condenser, which combined counteract the load imparted on the circuit by the test chamber. The FF rig test chamber houses the tubes which were tested individually in pool boiling mode in this study. Liquid refrigerant was boiled by the testing tube through heating water passing through the inside of the tube. The resulting refrigerant vapour from this boiling process exits the top of the test chamber and goes to on overhead condenser, which after being condensed falls down to the lower level of the rig which acts as a refrigerant reservoir. Here the electrical kettle evaporator heats the liquid back to saturation temperature, whereafter the variable speed refrigerant pump returns the liquid to the test chamber at a controlled flow rate.

2.2. Test chamber

The test chamber, as shown in the schematic of Figure 2-1 (b), was configured for the pool boiling setting and has internal dimensions of 566 × 650 × 69 mm, and provides the testing environment for pool boiling. The individually tested tubes were submerged in saturated refrigerant within the test chamber and, except for the movement induced by the boiling itself, the fluid was stationary. The untested tubes in the stack are insulated at the ends to reduce external influence on the test chamber.

The liquid refrigerant enters at the top of the chamber to submerge the tested tube in a liquid pool. The liquid pool level height was measured using the pressure differential between the bottom and top transducers and the hydrostatic formula, and was automatically controlled to a constant level with a proportional–integral–derivative (PID) control system linked to the feed rate of the refrigerant gear pump. The pool was controlled to be 40 ± 10 mm above the tested tube. In the pool boiling configuration as seen in Figure 2-1 (b), all the chamber valves are closed except for the top valve where refrigerant vapour can rise and exit to the overhead condenser.

A specialized thermocouple rod containing 3 equidistant, opposite extending pairs of type K thermocouples and covering a 554 mm span was situated inside the tested tube and used to measure the heating water temperature profile along the length of the tube. A polynomial fit of the temperature profile was used obtain the mid-point temperature gradient and thus heat flux of the tube. This thermocouple rod has copper wire wrapped around its length to serve as a water mixer.

There are Endress+Hauser PMC 731 pressure transducers at the top and bottom of the testing chamber which measure the pressure and compare the saturation pressure to the calculated saturation pressure based on the K-type thermocouples situated around the testing chamber to ascertain that no affecting non-condensable gases are present in the system. In this study the difference between the saturation temperature measured directly from the thermocouples and that calculated from the saturation pressure was less than 0.2°C, indicating the vacuuming process used during the charging of the rig was successful in ensuring minimal presence of non-condensable gases.

All pool boiling experiments were visually observed through 6 glass windows on either side of the testing chamber. A Photron FASTCAM Mini UX100 [16], set to record at 2 000 frames per second (fps), was additionally used for this study with a Tokina 100 mm f/2.8 AT-X PRO 1:1 Macro lens.

2.3. Test Procedure

All tests were conducted in R134a refrigerant at a saturation temperature of 5°C under pool boiling conditions. Given the lack of experimental data for the EHPII and GEWA-KS tube in open literature, these surfaces were also tested at 25°C. This also assisted in understanding the influence of changes in operating pressure on the heat transfer processes of these multiscale surfaces.

The pool boiling tests consisted of varying the temperature of the heating water so that the heat fluxes range from a high of 100 kW/m^2 to a low of 20 kW/m^2 in increments of 10 kW/m^2, with this decreasing heat flux ensuring quicker initial facility stabilisation. Comprehensive boiling hysteresis studies were not conducted for this study, but previous work by the authors on plain tubes noted boiling hysteresis to only occur below approximately 5 kW/m^2 for R-134a and so was not a focal point for this study. Heat fluxes and external heat transfer coefficients (HTCs) were recorded at the midpoint of the tube.

2.4. Tube samples

2.4.1. Tubes tested

This study was conducted on one plain roughened tube and three commercially micro-enhanced tubes all with nominal ¾" (approximately 19 mm) diameter and a heated length of 566 mm, with one low finned GEWA-KS with 19 fpi tested, and two '3D enhanced' re-entrant cavity style tubes tested, the Turbo EHPII and the GEWA-B5. Key tube dimensions are presented in Table 1:

Table 1. Tested tubes diameters

Tube	D_o **[mm]**	D_{or} **[mm]**	D_i **[mm]**
Roughened	19.1	19.1	16.7
GEWA-B5	18.8	17.4	16.0
GEWA-KS	18.8	17.2	14.9
EHPII	18.9	18.6	16.0

Schematic representations of the surfaces are depicted in Figure 2-2. The surface of the EHPII tube, illustrated in Figure 2-2 (b), is made to appear like scales slotted into each other. The GEWA-B5 microstructured illustrated in Figure 2-2 (b) comprises mushroom-like pin fins to form a network of re-entrant cavities. All of the enhanced tubes have inner enhancements to boost the internal convective heat transfer. The influence of these enhancements is categorized through a Wilson plot methodology.

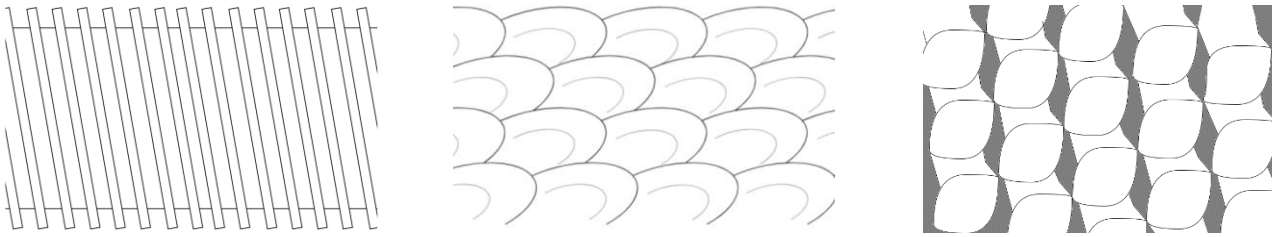

(a) GEWA-KS (b) EHPII (c) GEWA-B5

Figure 2-2. Surface microstructure schematics of tubes tested

2.4.2. Uncoated tubes

All the tubes tested were of nominal ¾" outside diameter (19 mm) and 568 mm long. The uncoated tubes were initially prepared with a standardised cleaning procedure. The tubes were fully submerged in a weak 5% acidity acetic

acid solution for 1 hour to clean the surface. The tubes were exposed to still atmosphere to age for 12 hours after which they were rinsed with Reverse Osmosis (RO) water and acetone. The procedure to nanocoating CuO on copper was derived from the outline given by Enright et al. [27]. Furthermore, the roughened plain tube was prepared with grit 40 sandpaper by dry sanding the tubes longitudinally by hand. The sanding of the tubes mechanically removes the surface sediments and copper carbonate layers and thus they were also aged in atmosphere and rinsed afterwards with RO water and acetone. Surface roughness of the rough tube was measured on a flat copper plate that was sanded with the same relative intensity as the tube with a Mitutoyo SJ 210 Surftest Profilometer using the ISO 1997 standard and a cut-off length of 0.8 mm which resulted in a roughness average value (R_a) of 0.75 μm with a standard deviation of 0.07 μm. It should be noted that the surface roughness's measured in this study did not match those measured in Bock [16] where the same grit sandpapers where used, which highlights the influence of the user on the intensity of a manual sanding process.

2.4.3. Coated tubes

A set of micro-enhanced tubes and a roughened tube were surface coated with a copper oxide (CuO) nanocoating. The tubes to be coated were prepared according to a specific set of consistent steps to ensure that the same CuO was produced on each tube. The CuO Type I nanocoating of Nam and Ju [28] and Enright et al. [27] was used in this study. The chemicals used for the coating process are summarised in Table 2, indicating the constituent proportions in weight percentage:

Table 2. Chemicals for CuO coating constituent weight percentages in solution

Chemical	**Weight [%]**
$NaClO_2$	3.75
NaOH	5
$Na_3PO_4{\cdot}12H_2O$	10
H_2O	100

The chemical coating event is a 2-step process where Copper (I) oxide is first produced which then binds with the free suspended hydroxide ions within the solution to produce Copper (II) oxide [27, 28]. The resultant CuO nanostructures on the surface are described as having sharp-like point structures with prominent blade protrusions throughout the nanocoating with an approximate height of 1 μm, blade width of 300 nm and a blade thickness of 100 nm [27, 29]. At certain pH values there should be different visible elements that constitute the nanostructures which consist of CuO nanorods at pH = 8, CuO nanosheets at pH = 10 and CuO nanoflowers at pH = 11 [30]. The pH of the coating solution estimated to be pH = 12.56. With this, all the nanostructure elements should be present in the resultant coating. This is verified with their identification in Figure 2-3 from a scanning electron microscope (SEM) image taken of one the surfaces coated.

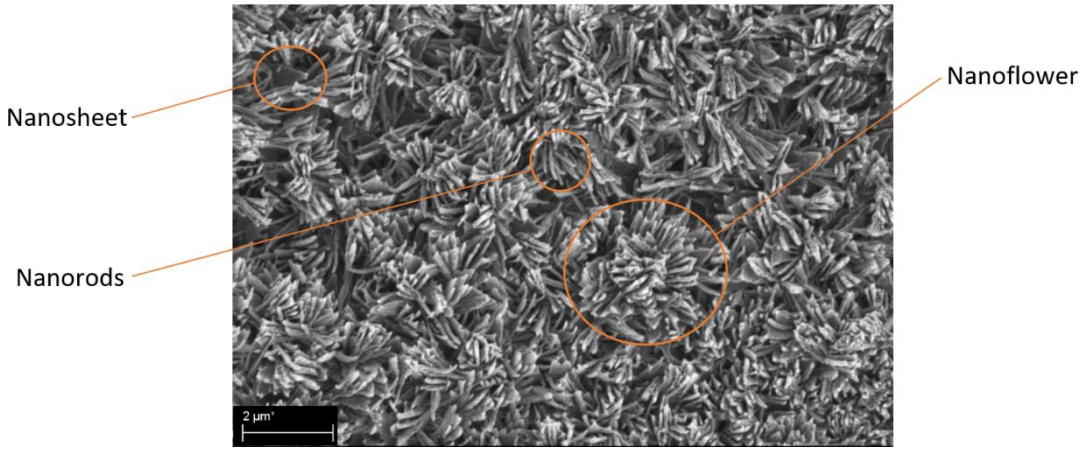

Figure 2-3. Nanostructure identification on SEM photograph of CuO nanocoated copper sample

The thermal conductivity of CuO is estimated to be as low as 33 W/mK [31]. However, by comparing the thermal resistances of the CuO nanocoating to that of a plain copper tube wall, it was estimated that the CuO coating only increases the wall thermal resistance by 1.2% due to it being a very thin coating (cross sections suggest a thickness of only 1.5 µm [16, 27] and is thus not a significant factor to consider regarding its influence on heat transfer.

The coatings on all the micro-enhanced tubes were investigated with SEM. It was determined that a uniform nanocoating along the profile of the micro-enhanced tube surface was achieved without any significant clogging nor obstruction of the microstructures. Since the CuO is extremely non-conductive it causes the surface to charge up with electrons when subjected to the electron beam in the SEM so that it cannot successfully render a true image. The samples were first coated with a thin layer of carbon using a Quorum Q150T ES Carbon Coater and vaporizing pure carbon sticks in a sealed vacuum chamber to alleviate this problem. The deposited conductive layer does not affect the nanostructures beneath, but merely makes them possible for viewing. The uncoated and coated tubes comparisons through SEM micrographs are shown in Figure 2-4.

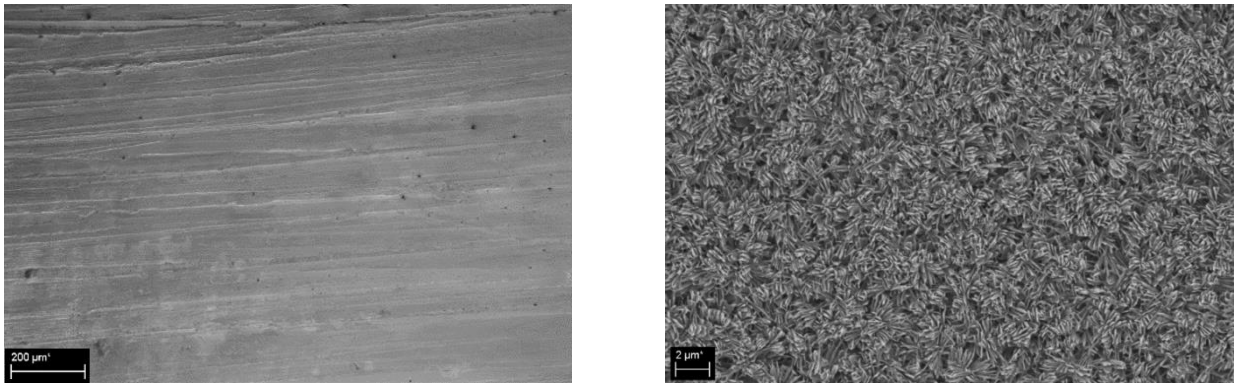

(a) Roughened uncoated (b) Roughened coated

Figure 2-4. Uncoated and coated micro-enhanced tube SEM observation

Some blockages of the EHPII microstructure pores did occur and consisted of a sponge-like webbing across the pores. It is also observed that the blockages are not at every crevice, where an estimated 12.5% of all scales have these blockages. Whether these seemingly delicate webbings draped across the pore openings would survive the vigorous boiling process is also debatable, but was not confirmed in this study. From the SEM images shown in Figure 2-4, the nanocoating could uniformly cover the entirety of the intricate surfaces, including the GEWA-B5 and EHPII tubes. This characteristic of the CuO nanocoating was attributed to the self-limiting nature by which the nanocoating solution binds with the copper surface, preventing a thick coating from forming.

The wettability of the surfaces was also thought to be enhanced. This was explored by water droplet contact angle (CA) tests on all the tubes. The hydrophobic uncoated tubes produced water droplet CAs between 60° to 80°, where the super hydrophilic CuO nanocoated tubes produced water droplet CAs of less than 5°. Furthermore, the CuO

coating SEM images visually coincide with the CuO nanostructure SEM images captured by Sen et al. [13], who investigated hydrophilic and hydrophobic CuO nanostructure coated copper surfaces, suggesting a hydrophilic coating was achieved.

2.5. Data reduction

The detailed data reduction, procedures, uncertainty calculations and the Wilson plot for the FF rig were described by Habert [32]. Only the principal quantities are described here in brief.

2.5.1. Local heat flux

The local heat flux calculated at the centre of the tube length was used to determine the local HTCs at that point. Equation (1) was used to calculate heat flux:

$$\dot{q} = \frac{\dot{m}_w \cdot c_{p,w}}{\pi \cdot D_o} \cdot \frac{dT_w}{dx} \tag{1}$$

Where $\dot{m}_w$ denotes the measured heating water mass flow rate and D_o the nominal tube outside diameter.

A 2nd degree polynomial fit was applied to the temperatures measured along the length of the tube to obtain the temperature profile $\frac{dT_w}{dx}$. The specific heat capacity, $c_{p,w}$, and all other thermophysical properties, were estimated using CoolProp v.6.4.1 open-source module.

2.5.2. Overall heat transfer coefficient relative to outside tube surface

The local midpoint overall HTC, $U_{o,mid}$, is calculated from equation (2), using the calculated refrigerant saturation temperature, $T_{r,sat}$:

$$U_{o,mid} = \frac{\dot{q}_{o,mid}}{T_{r,sat} - T_{w,mid}} \tag{2}$$

Where $\dot{q}_{o,mid}$ is the heat flux evaluated at the middle of the tube via a 2nd degree polynomial fit applied to the temperature profile obtained along the tube length, $T_{r,sat}$ being the theoretically calculated refrigerant saturation temperature and $T_{w,mid}$ the heating water temperature at the middle of the tube.

2.5.3. Internal heat transfer coefficient

The internal heat transfer coefficient is calculated using a modified Gnielinski correlation by altering the leading coefficient C_i through a Wilson plot analysis to account for the inner tube enhancements and the presence of the tube mixer. The internal heat transfer coefficient was therefore calculated in equation (3):

$$h_i = Nu^*_{Gnie} \cdot \left(\frac{k_w}{D_h}\right) \tag{3}$$

Where D_h denotes the hydraulic diameter of the inside tube to accommodate effects of the thermocouple probe diameter inside the testing tube k_w being the water thermal conductivity.

The modified Gnielinski correlation, Nu^*_{Gnie}, was used as described in (4):

$$Nu^*_{Gnie} = C_i((f/8)(Re_w - 1000)Pr_w)/(1 + 12.7(f/8)^{0.5}(Pr_w^{2/3} - 1)) \tag{4}$$

The friction factor was calculated with Petukhov's formulation [33], while C_i is the internal Wilson plot coefficient to characterise the internal heat transfer effects and modify the Gnielinski correlation accordingly.

The Wilson plot coefficient, C_i, for each tube tested is shown in Table 3. As can be seen, the 3D enhanced tubes have the highest internal Wilson plot coefficient and highest internal heat transfer due to the advanced helical structures present on the inner tube surface.

Table 3. Wilson plot coefficients for tubes

Tube	Wilson plot coefficient, C_i
Plain roughed	1.28
GEWA-KS	3.91
GEWA-B5	4.20
EHPII	4.48

2.5.4. Thermal wall resistance

The resistance to heat transfer the wall poses was calculated through equation (5):

$$R_t = \frac{D_o \cdot \ln\left(\frac{D_{or}}{D_i}\right)}{2 \cdot k_t} \tag{5}$$

Where k_t is the estimated thermal conductivity of copper, and was taken as k_t of 340 W/mK [34].

2.5.5. Outside tube surface heat transfer coefficient

Considering the thermal network and when normalized to outside tube surface area, the external heat transfer coefficient, h_o, is given by equation (6):

$$h_o = \left(\frac{1}{U_{o,mid}} - R_t - \frac{1}{h_i} \cdot \frac{D_o}{D_i}\right)^{-1} \tag{6}$$

Where $U_{o,mid}$ is the determined overall heat transfer coefficient with respect to the middle of the tube, R_t the calculated thermal wall resistance, h_i the determined internal heat transfer coefficient and D_o and D_i the respective outer and inner diameter of the tube.

2.5.6. Heat flux exponent

The influence of heat flux are quantified by equation (7):

$$h_o = a \cdot \dot{q}^{n_q} \tag{7}$$

2.5.7. Enhancement heat transfer influence ratio

The effect of the 3D surface enhancements on heat transfer were observed through a ratio of the heat transfer coefficients of the microstructured tube to those of the plain roughened tube at the same testing heat flux point. This was done by calculating a polynomial best-fit curve to each of the heat transfer curves and dividing the HTCs of each of the micro-enhanced tubes by the HTCs of the plain roughened tube over the testing heat flux range in intervals of 10 kW/m2. This ratio, K_{surf}, was calculated for both uncoated and coated cases as in equation (8):

$$K_{surf} = \frac{h_{enhanced}}{h_{roughened}} \tag{8}$$

2.5.8. Coating heat transfer influence ratio

The heat transfer influence the CuO coating imposes on HTCs was quantified as the ratio of the heat transfer performance of the CuO coated tube, $h_{o,CuO}$, to the heat transfer performance of the same uncoated tube, h_o at the same heat flux and refrigerant conditions. The calculation was performed by fitting a polynomial equation to the h_o data to obtain a HTC at the same heat flux as that of the $h_{o,CuO}$ data . This ratio is defined as K_{CuO} and is given by equation (9):

$$K_{CuO} = \frac{h_{o,CuO}}{h_o} \tag{9}$$

2.6. Uncertainty

The uncertainties of temperature probes were found to be 0.1 K, and the pressure and mass flow rate probes were found to be 0.2%, and all were calculated according to the uncertainty analysis techniques by Dunn [35] which accommodates the acquired bias and precision in calculating probe uncertainty. The uncertainties of calculated quantities were determined using the 'Law of Propagation of Uncertainty' as described by JCGM 100:2008 [36], with the full derivation of these calculation found in Bock [37]. The maximum and minimum uncertainties of the key calculated quantities are summarized in Table 4, with the average across all points measured also shown:

Table 4. Summary of all pool boiling heat flux and HTC uncertainties

	Overall average uncertainty [%]	**Average uncertainty at 20 kW/m² [%]**	**Average uncertainty at 100 kW/m² [%]**
q	10.7	21.7	7.0
h_o	24.4	48.1	16.3
K_{CuO}	5.1	14.8	1.6

The behaviour of the uncertainties of the quantities contained in Table 4 is illustrated through Figure 2-5, where the higher uncertainty percentages are expected at the lower heat flux range. This study makes use of ratios to aide analysis, as these ratios are calculated using the same measurement sensors and so have correlated inputs [37] and as such lower uncertainties. For example, the uncertainty of the coating heat transfer influence ratio, K_{CuO}, has typically single digit uncertainties across most of the heat flux range.

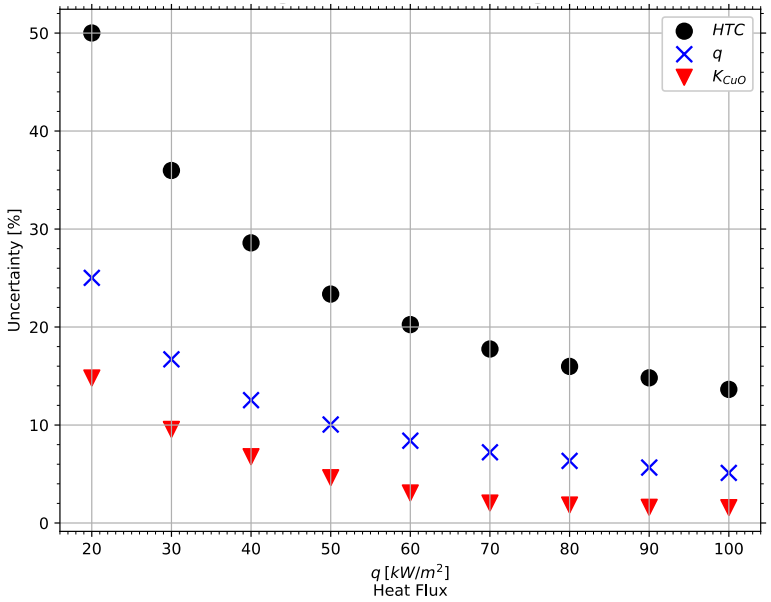

Figure 2-5. Percentage uncertainties under pool boiling in 5°C R134a

3. Validation

Condensation tests were conducted on a plain smooth tube that has been sanded by hand with 1200 grit sandpaper at 30°C saturation temperature R134a to validate the results from the FF Rig. The results agreed well with Nusselt's solution [38], with 91% of the smooth tube HTCs within 5% of the Nusselt solution. Furthermore, the results were found to generally be in reasonable alignment to other research data [16].

Pool boiling tests were also performed using a plain tube that was prepared to relate to previous researchers' tested samples. The Cooper correlation [39] and the Gorenflo and Kenning Model [40] were also compared to the pool boiling results. The accuracy of the Cooper correlation [39] was investigated by Ji et al. [41] to deduce its credibility to measure against. Figure 3-1 illustrated pool boiling results conducted on a smooth tube (Ra = 0.04 μm) with its

Cooper correlation [39] and Gorenflo and Kenning Model [40] ; Bock [37] with a smooth tube (Ra = 0.12 µm) with its Cooper correlation [39] for determination of its validity; and Ji et al. [41] with a tube of an assumed roughness of Ra = 0.3 µm.

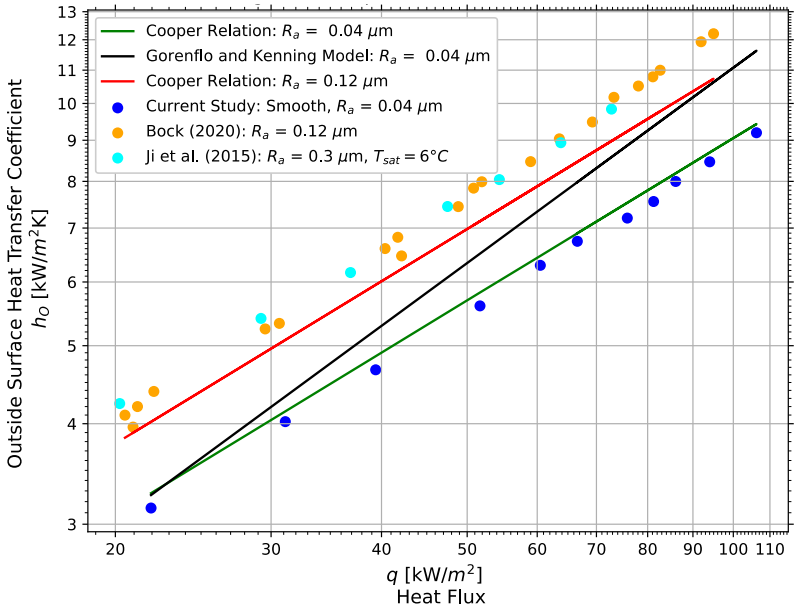

Figure 3-1. Smooth tube pool boiling validation test in R134a at 5°C

With this, it is established in Figure 3-1 that there are many influences on pool boiling HTCs yet to be properly researched and documented, leading to a general lack in consistency in pool boiling results among studies. This is especially observed above where Ji et al. [41] and Bock [37] produced approximately the same results where the surface tube roughness of Bock [37] is about half of Ji et al. [41].
It is seen that the data from the current study matches the Cooper correlation [39] well with an average deviation of 3.3%, where no divergence takes place across the heat flux range. The Gorenflo and Kenning Model [40] related very well in the beginning but diverged significantly (up to 17%) with increased heat flux. These results support the findings the by Li and Hrnjak [42] and discovered by Gorenflo et al. [43], that the Gorenflo and Kenning model [40] is more accurate at lower heat fluxes, and that a greater investigation into the thermophysical properties, especially surface tension, of the working fluid need to be incorporated into the models for industrial pool boiling applications.
The same trends regarding the Cooper [39] and Gorenflo and Kenning Model [40] in Figure 3-1 can be seen regarding the initial high accuracy and divergence in a comparative study performed by Sajjad et al. [44].
The lower HTCs from the current study compared to Bock [37] were most likely due to the lower surface roughness, with the Cooper correlation [39] using an input of 0.04 µm and 0.12 µm illustrating this.
The condensation and pool boiling results were considered to show sufficient agreement to consider the facility validated.

4. Results and discussion

4.1. Uncoated

The uncoated tubes were tested in pool boiling at saturation temperatures of 5°C and 25°C in R134a across a range of heat fluxes and their HTCs are found in Figure 4-1.

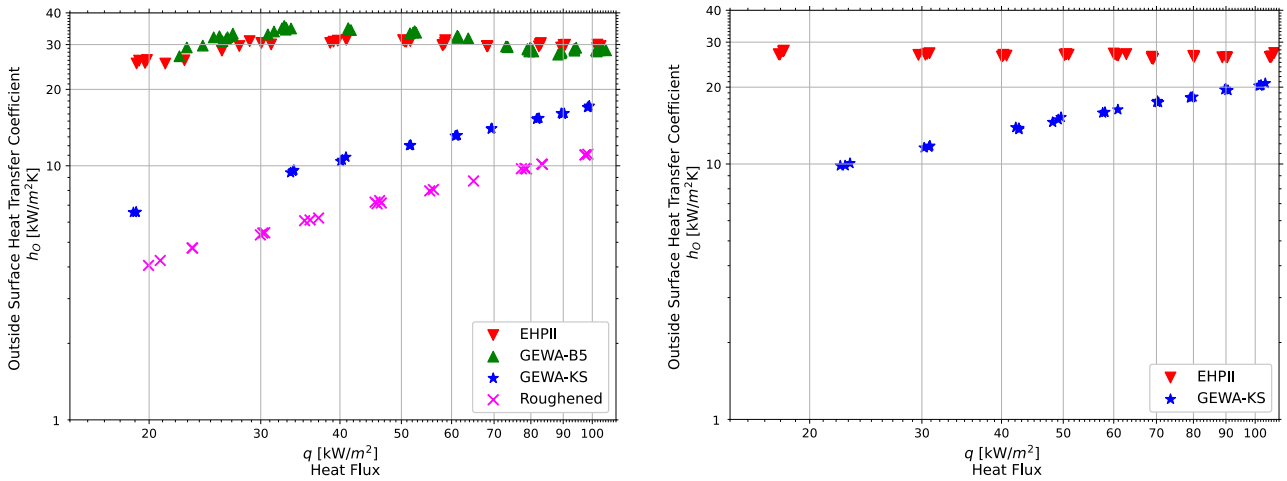

(a) 5°C (b) 25°C

Figure 4-1. Pool boiling HTCs of uncoated micro-enhanced tubes in R134a

It is observed in Figure 4-1(a) at 5°C that the 3D enhanced tubes performed the best followed by the low finned tube and then the roughened tube. The roughened tube HTCs increased by about 175% across the heat flux range and the GEWA-KS tube increased by about 160% across the heat flux range. This is typical for simple plain surfaces such as these, with increases in heat flux resulting from progressively more active nucleation sites being activated by the higher wall superheats.

The EHPII tube and the GEWA-B5 tube meanwhile had little dependence on heat flux. This insensitivity to heat flux has been noted before in other 3D enhanced re-entrant cavity style tubes [45, 46] with some cases showing a plateau region for only portions of the heat flux range tested [47, 48]. This is thought to be due to the complex interaction between the liquid flowing within the network of microchannels on the surface of these tubes and the vapour emerging from the nucleation sites, with greater vapour clogging [48] or internal dryout [46] possibly occurring as heat fluxes are increased, so counteracting any further improvements in heat transfer.

The EHPII and GEWA-KS tubes in 25°C saturation temperature performed similar to the 5°C saturation temperature case, but where the GEWA-KS HTCs improved, the EHPII HTCS slightly declined. The EHPII tube persisted with little dependence on heat flux with a decrease in HTC of -1.18% over the testing heat flux range, whereas the GEWA-KS tube with a 13.8% increase in HTCs. The EHPII tube's HTCs average deviation of -10% compared to the 5°C saturation temperature case indicates a minor decline in heat transfer performance, whereas the GEWA-KS with an average improvement of 25.5% compared to the 5°C saturation temperature shows greater improvement with an increase in saturation temperature.

4.2. Coated

The same pool boiling test was repeated for the CuO nanocoated tube sets shown in Figure 4-2. Heat transfer data for CuO nanocoated commercial tubes are non-existent for comparison at the time of writing.

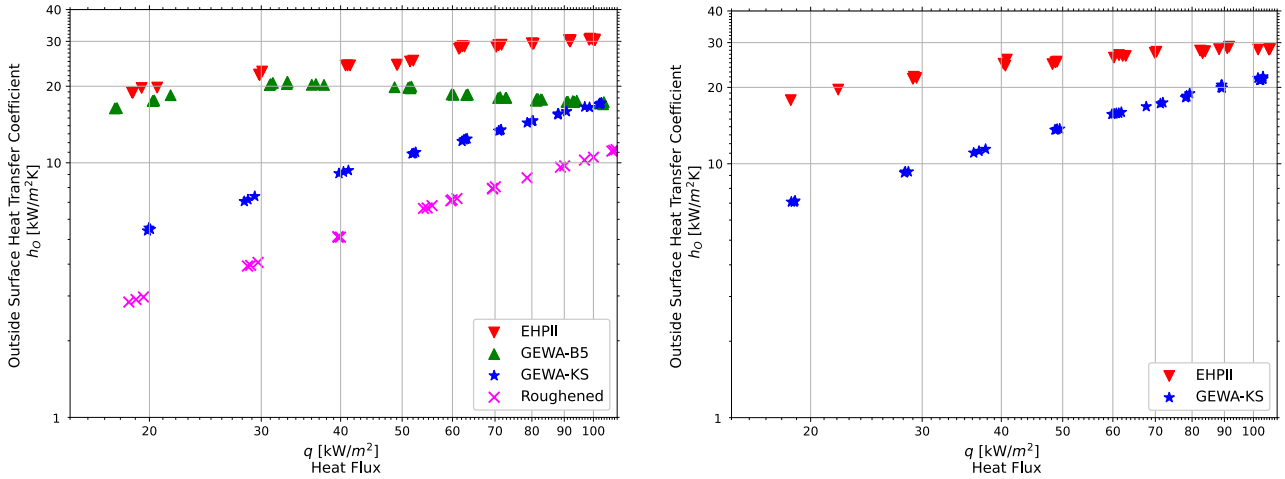

(a) 5°C (b) 25°C

Figure 4-2. Pool boiling HTCs of coated plain and micro-enhanced tubes in R134a

As seen in Figure 4-2 (a) for a 5°C saturation temperature, the HTCs of the coated EHPII tube and the GEWA-B5 tube significantly performed better than the GEWA-KS tube followed by the roughened tube. As with the uncoated case, the HTCs of the GEWA-KS and roughened tube increased linearly on the log-log plot. With an increase in saturation temperature, it was seen in Figure 4-2 (b) for a 25°C that the coated EHPII tube had an increase in HTCs of 60% and the GEWA-KS tube with an overall increase of 210% across the heat flux range. Furthermore, increasing the saturation temperature from 5°C to 25°C, the same behaviour is seen where the coated EHPII tube's HTCs decreased overall by about 3.4% while the coated GEWA-KS tube's HTCs increased overall by about 30%.

4.3. Influence of heat flux

The influence of heat flux was characterised through the exponents of the relation $h_o = a \cdot \dot{q}^{n_q}$ of the uncoated and nanocoated tubes and are listed in Table 5.

Table 5. Heat flux exponents of uncoated and nanocoated tubes

		Uncoated	**Coated**
Saturation Temperature [°C]	**Tube**	n_q	n_q
5	EHPII	0.06	0.29
	GEWA-B5	-0.10	-0.04
	GEWA-KS	0.57	0.69
	Roughened	0.61	0.78
25	EHPII	-0.02	0.23
	GEWA-KS	0.48	0.66

Table 5 indicates that the CuO nanocoating influenced the surface boiling mechanics to generally increase the boiling exponent n_q so that the HTCs have a greater sensitivity to changes in heat flux.. The boiling exponent of the roughened tube and the GEWA-KS tube, both of which can be considered plain surfaces, are lower than the plain tube boiling exponents of 0.67 used by Cooper [49] or the 0.81 predicted by Gorenflo et al. [43], but the Gewa-KS exponent did decrease as the reduced pressure was increased from 5 to 25°C, in line with the trend predicted by Gorenflo et al.'s [43] correlation. The exponents of the 3D enhanced tubes are close to zero, highlighting their insensitivity to changes in heat flux across the range tested in this study.

4.4. Influence of enhancements

The ratio of the HTCs of the enhanced tubes to that of the plain roughened tube used in this study were calculated at 5°C in R134a in order to investigate the effect of the surface enhancements over the plain roughened surface with respect to heat transfer and is illustrated in Figure 4-3.

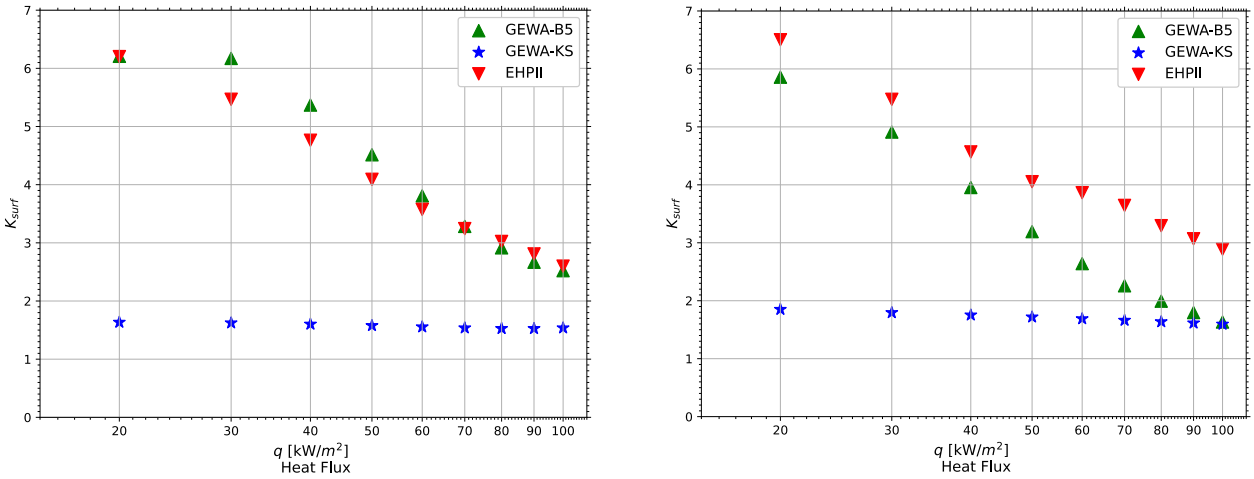

(a) Uncoated (b) Coated

Figure 4-3. Surface enhancement ratio with respect to the plain roughened tube at 5°C in R134a

It is shown in Figure 4-3 that the intricate enhancements on the micro-enhanced tubes greatly increased the heat transfer performance compared to the plain tube, where both the GEWA-B5 and the EHPII tube performed similarly when uncoated in Figure 4-3(a) where the minimum enhancement was at 100 kW/m² with a factor of 2.5 and a maximum enhancement of 6.2 at 20 kW/m², where the 2 points had a linear trend.

The GEWA-KS had a fairly constant enhancement ratio of around 1.6 to 1.9 in both the uncoated and coated case. The GEWA-KS has approximately 1.8 times the area of a plain tube of same nominal diameter [50] and thus the simple low fin enhancements mainly improves heat transfer through the provision of a higher effective heat transfer surface area.

4.5. Influence of the CuO coating

The coating heat transfer influence ratios, K_{CuO}, of all the pool boiling cases were calculated and are collectively presented in Figure 4-4. The HTC enhancement or deterioration are described through a K_{CuO} factor respectively greater or smaller than 1.

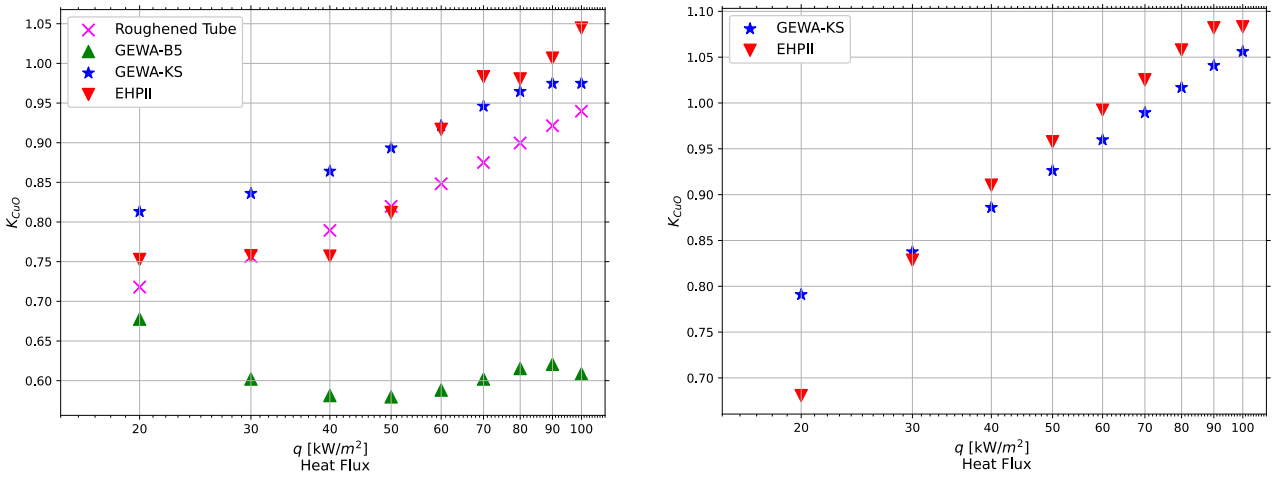

(a) 5°C (b) 25°C

Figure 4-4. Coating heat transfer influence ratios of the plain and micro-enhanced tubes in R134a

The CuO coating did not improve HTCs on the roughened tube with an average K_{CuO} of 0.85 across the range of heat fluxes tested. The CuO nanocoating on the GEWA-KS low fin tube is observed in Figure 4-4 to have had minimal influence on heat transfer where the average K_{CuO} value was 0.91 for a 5°C saturation temperature and 0.95 for a 25°C saturation temperature. With the average K_{CuO} values being slightly lower than 1, heat transfer is only slightly diminished. The coated GEWA-B5 tube had HTC ratios from 0.7 to 0.58 of those of the uncoated GEWA-B5 tube and an average K_{CuO} of 0.6. It was therefore influenced the most by the coating where it previously performed with HTCs 318% greater than those of the roughened plain tube in the uncoated case. The CuO nanocoating on the EHPII tube is seen not to have a great impact on the heat transfer where the average K_{CuO} was 0.89 for the 5°C saturation temperature case and a slightly higher 0.97 for the 25°C case.

At high heat fluxes, the HTCs were seen to be unchanged at 5°C but were slightly enhanced at 25°C. However, at low heat fluxes, the coating lowered heat transfer performance with the K_{CuO} value being as low as 0.7 for both saturation temperatures. The general upward trends of the K_{CuO} values for both saturation temperatures in Figure 4-4 suggest further investigation of possible greater heat transfer enhancement at very high heat fluxes outside of those tested may be possible.

The worst result from the coating was found in the case of the GEWA-B5 tube, where the HTCs were almost halved. This merited further visual inspection of the boiling phenomena on the uncoated and coated GEWA-B5 tubes to understand the reasons for this. Figure 4-5 illustrates high speed images of the GEWA-B5 tube at 100kW/m^2 in R134a at a 5°C saturation temperature.

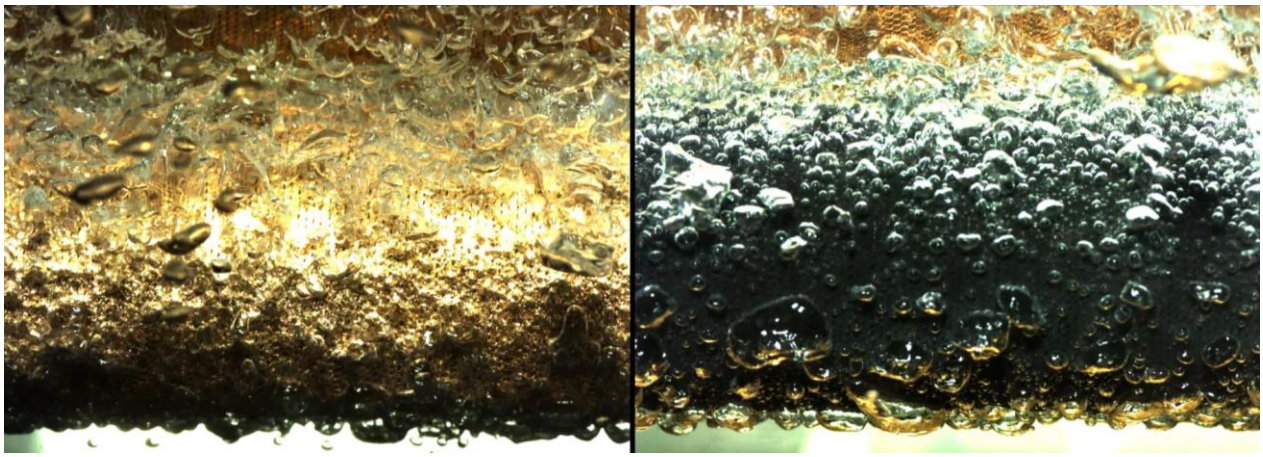

(a) Uncoated (b) Coated

Figure 4-5. Images of pool boiling of uncoated and coated GEWA-B5 at 5°C in R134a at 100kW/m^2

Figure 4-5 illustrates that the nucleation process itself appears diminished resulting in a general lower bubble density on the surface of the coated tube compared to the uncoated tube. From visual inspection of the high speed vide it also appears that the coated CuO tube had slower bubble development and ejection, although it was not possible to quantify this meaningfully from the images obtained.

A further likely contribution to the diminished heat transfer is that the coated GEWA-B5 seemed to have non-periodic bubble generation and slow nucleation at the micro-channel crevices, where substantial vapour entrapment occurred within these crevices. This is illustrated in Figure 4-6, where the GEWA-B5 is boiling at 20 kW/m^2 and instances of this entrapment are indicated with red circles, where bubbles can be seen to be trapped within the re-entrant cavities. The uncoated GEWA-B5 tube meanwhile boiled as expected, where the active nucleation sites produced bubbles that were ejected from micro-channel crevices followed by a new bubble in periodic fashion.

Figure 4-6. Bubble ejection impedance in coated GEWA-B5 re-entrant cavities in pool boiling at 20kW/m^2 and 5°C in R134a

This entrapped vapour seen in Figure 4-6 in the crevices was prominent and pulsated, with an occasional build up and release of a large bubble from a cavity. It appears that the bubbles were kept in place by the overhangs of the re-entrant cavities without the aid of a superheating microlayer for the bubble to rapidly grow and overcome the liquid surface tension. This behaviour of the coated surface was present at higher heat fluxes too. It is likely thus that part of the heat transfer performance loss can be attributed to this behaviour of the coated surface, where bubble release is hindered and a portion of the internal surfaces of the cavities could be covered by a vapour lining, preventing the micro-channels from enhancing nucleation heat transfer. The extent of this is unfortunately unknown, as this is not visible from the video as it is hidden within the micro-enhancements.

Lastly, as the reduction in heat transfer performance may be due to the disruption of the GEWA-B5 enhanced heat transfer mechanism within its re-entrant cavity network. The interconnected re-entrant cavities are thought to significantly enhance heat transfer as liquid is drawn through these channels by the 'pumping' caused by bubble departure from nucleation sites [37]. This mechanism have been disrupted by the reduced ejection of bubbles from the re-entrant cavities leading to a weaker bubble pumping action at the cavity openings causes for an overall slower fluid movement through the micro-channel network and thus less sensible heat transfer.

Furthermore, the presence of the rough and hydrophilic CuO coating on the interior of the re-entrant cavity network may have posed greater resistance to general liquid flow within the micro-channels. This complements the deductions made by Jin et al. [8] in their study where a hydrophobic chlorofluoro coating was applied to commercially micro-enhanced boiling tubes and where found to enhancement heat transfer, which was thought to be caused by the low surface energy nature of the coating reducing the friction within the microchannels, allowing for increased fluid flow and easier elimination of vapour from these channels.

These findings thus suggest that the hopes of reduced dryout within the microchannels and subsequent improved heat transfer were not realised because of the hydrophilic coating and any possible are overpowered by the disruption to the enhanced boiling process. The hydrophobic surfaces thus appear to be more promising approach to multiscale enhancement of commercially produced micro-enhanced tubes, as seen in the work of Jin et al. The CuO coating used in this study may itself be modified to have a hydrophobic nature by altering the reagents or their concentrations during coating [12].

5. Conclusion

This study experimentally investigated the ability of multiscale physical enhancements to enhance refrigerant pool boiling HTCs through the addition of a wickable CuO nanocoating to commercially produced microstructured tube surfaces in the hope of combining the two sets of beneficial heat transfer mechanisms the two scales of enhancement have previously seen to provide. For the first time, uncoated and CuO nanocoated sets of roughened, low finned GEWA-KS, and 3D enhanced re-entrant cavity GEWA-B5 and EHPII tubes were tested under pool boiling of R134a at saturation temperatures of 5°C and 25°C across a heat flux range of 20 kW/m^2 to 100 kW/m^2.

The study's analyses lead to the following valuable points:

1. The uncoated enhanced tubes performed well against the uncoated roughened tube, with the HTCs of the low finned GEWA-KS up to 64% greater, the EHPII tube up to 519% greater and the GEWA-B5 up to 539% greater than an uncoated plain roughened tube at 5°C.

2. The CuO nanocoating reduced heat transfer for all tubes tested at low heat fluxes, while at higher fluxes it had minimal impact. The average reduction factor across the heat flux range tested compared to the uncoated tubes was 0.85 for the roughened tube, 0.91 for the GEWA-KS, 0.89 for the EHPII, and 0.60 for the GEWA-B5 at 5°C.
3. The EHPII and GEWA-KS were tested at both 5°C to 25°C. This change had a minimal effect on heat transfer for the EHPII tube, while the GEWA-KS HTCs increased by between 15% to 30% as saturation temperature was increased.
4. The coated GEWA-B5 was noted to trap bubbles within the re-entrant cavity network, likely contributing to the decreased heat transfer seen.
5. The CuO nanocoating is likely to have degraded heat transfer the by reducing the nucleation sites on the plain surfaces. The 3D enhanced surfaces may have suffered from the rough coating reducing liquid flow within the re-entrant cavity network, as well as possible nucleation site reduction.

Considering the wide array of nanocoating's available, other coatings may have better success that the coating tested in this study. But coatings that produce high roughness's should be avoided on 3D enhanced tubes due to the expected heat transfer degradation seen in this study.

Credit authorship contribution statement

Dian Dickson: Formulation, validation, official examination, data management, writing and review, investigation.
Bradley D. Bock: Formulation, procedures, validation, official examination, writing and review, project management, finances, supervision, resources provision.
John R. Thome: Conceptualisation, procedures, validation, writing, review and editing.

Declaration of competing interest

The authors declare no conflict of interest.

Acknowledgements

The authors express their gratitude to the Renewable Energy Hub and Spokes Programme of the Department of Science and Innovation (DSI), and Wieland Group for the supply of the tubes tested.

References

[1] H. J. Lombard, "SMALL SOLAR ORGANIC RANKINE CYCLE FOR ELECTRICITY GENERATION," Mechanical Engineering, Department of Mechanical and Mechatronic Engineering Stellenbosch University, Stellenbosch, 2015.

[2] P. Lu *et al.*, "Design and Optimization of Organic Rankine Cycle Based on Heat Transfer Enhancement and Novel Heat Exchanger: A Review," *Energies,* vol. 16, no. 3, 2023, doi: 10.3390/en16031380.

[3] V. R. Patil, V. I. Biradar, R. Shreyas, P. Garg, M. S. Orosz, and N. C. Thirumalai, "Techno-economic comparison of solar organic Rankine cycle (ORC) and photovoltaic (PV) systems with energy storage," *Renewable Energy,* vol. 113, pp. 1250-1260, 2017/12/01/ 2017, doi: https://doi.org/10.1016/j.renene.2017.06.107.

[4] C. M. Kruse *et al.*, "Enhanced pool-boiling heat transfer and critical heat flux on femtosecond laser processed stainless steel surfaces," (in en), *International Journal of Heat and Mass Transfer,* vol. 82, pp. 109-116, 03/2015 2015, doi: 10.1016/j.ijheatmasstransfer.2014.11.023.

[5] A. Joseph *et al.*, "An experimental investigation on pool boiling heat transfer enhancement using sol-gel derived nano-CuO porous coating," (in en), *Experimental Thermal and Fluid Science,* vol. 103, pp. 37-50, 05/2019 2019, doi: 10.1016/j.expthermflusci.2018.12.033.

[6] G. Liang and I. Mudawar, "Review of pool boiling enhancement by surface modification," *International Journal of Heat and Mass Transfer,* vol. 128, pp. 892-933, 2019/01/01/ 2019, doi: https://doi.org/10.1016/j.ijheatmasstransfer.2018.09.026.

[7] Y. Im, C. Dietz, S. S. Lee, and Y. Joshi, "Flower-Like CuO Nanostructures for Enhanced Boiling," *Nanoscale and Microscale Thermophysical Engineering,* vol. 16, no. 3, pp. 145-153, 2012, doi: 10.1080/15567265.2012.678564.

[8] P.-H. Jin *et al.*, "Liquid film boiling on plain and structured tubular surfaces with and without hydrophobic coating," *International Communications in Heat and Mass Transfer,* vol. 125, p. 105284, 2021/06/01/ 2021, doi: https://doi.org/10.1016/j.icheatmasstransfer.2021.105284.

[9] D. Attinger *et al.*, "Surface engineering for phase change heat transfer: A review," (in en), *MRS Energy & Sustainability,* vol. 1, no. 1, p. 4, 01/2014 2014, doi: 10.1557/mre.2014.9.
[10] C. G. Jothi Prakash and R. Prasanth, "Enhanced boiling heat transfer by nano structured surfaces and nanofluids," *Renewable and Sustainable Energy Reviews,* vol. 82, pp. 4028-4043, 2018/02/01/ 2018, doi: https://doi.org/10.1016/j.rser.2017.10.069.
[11] S. Massachusetts Institute of Technology. Center for Materials *et al.* (2014). Separate effects of surface roughness, wettability, and porosity on the boiling critical heat flux. Available: http://hdl.handle.net/1721.1/86912
[12] B. Köroğlu, K. S. Lee, and C. Park, "Nano/micro-scale surface modifications using copper oxidation for enhancement of surface wetting and falling-film heat transfer," *International Journal of Heat and Mass Transfer,* vol. 62, pp. 794-804, 2013/07/01/ 2013, doi: https://doi.org/10.1016/j.ijheatmasstransfer.2013.03.040.
[13] P. Sen, S. Kalita, D. Sen, S. Das, and A. K. Das, "Pool Boiling Heat Transfer on a Micro-Structured Copper Oxide Surface with Varying Wettability," (in en), *Chemical Engineering & Technology,* vol. 45, no. 5, pp. 808-816, 05/2022 2022, doi: 10.1002/ceat.202100558.
[14] G. Patel, S. S. Gajghate, A. Pal, U. Nath, S. Bhaumik, and S. Das, "Experimental investigation on nucleate pool boiling heat transfer enhancement for nano-structured copper oxide coated heating surface," (in en), *Journal of Physics: Conference Series,* vol. 1240, no. 1, p. 012093, 2019-07-01 2019, doi: 10.1088/1742-6596/1240/1/012093.
[15] X. Li, I. Cole, and J. Tu, "A review of nucleate boiling on nanoengineered surfaces – The nanostructures, phenomena and mechanisms," (in en), *International Journal of Heat and Mass Transfer,* vol. 141, pp. 20-33, 10/2019 2019, doi: 10.1016/j.ijheatmasstransfer.2019.06.069.
[16] B. D. Bock, "Surface influences on falling film boiling and pool boiling of saturated refrigerants: influences of nanostructures, roughness and material on heat transfer, dryout and critical heat flux of tubes," PhD Thesis, University of Pretoria, 2020.
[17] T. Kunugi, K. Muko, and M. Shibahara, "Ultrahigh heat transfer enhancement using nano-porous layer," (in en), *Superlattices and Microstructures,* vol. 35, no. 3-6, pp. 531-542, 3/2004 2004, doi: 10.1016/j.spmi.2004.04.002.
[18] S. Lee, B. Köroğlu, and C. Park, "Experimental investigation of capillary-assisted solution wetting and heat transfer using a micro-scale, porous-layer coating on horizontal-tube, falling-film heat exchanger," *International Journal of Refrigeration,* vol. 35, no. 4, pp. 1176-1187, 2012/06/01/ 2012, doi: https://doi.org/10.1016/j.ijrefrig.2011.11.015.
[19] K.-H. Chu, Y. Soo Joung, R. Enright, C. R. Buie, and E. N. Wang, "Hierarchically structured surfaces for boiling critical heat flux enhancement," (in en), *Applied Physics Letters,* vol. 102, no. 15, p. 151602, 2013-04-15 2013, doi: 10.1063/1.4801811.
[20] Y.-Q. Wang *et al.*, "Copper vertical micro dendrite fin arrays and their superior boiling heat transfer capability," (in en), *Applied Surface Science,* vol. 422, pp. 388-393, 11/2017 2017, doi: 10.1016/j.apsusc.2017.05.251.
[21] M. M. Rahman and M. McCarthy, "Boiling Enhancement on Nanostructured Surfaces with Engineered Variations in Wettability and Thermal Conductivity," (in en), *Heat Transfer Engineering,* vol. 38, no. 14-15, pp. 1285-1295, 2017-10-13 2017, doi: 10.1080/01457632.2016.1242961.
[22] P. Xu and Q. Li, "Visualization study on the enhancement of heat transfer for the groove flat-plate heat pipe with nanoflower coated CuO layer," (in en), *Applied Physics Letters,* vol. 111, no. 14, p. 141609, 2017-10-02 2017, doi: 10.1063/1.4986318.
[23] S. K. Singh and D. Sharma, "Review of pool and flow boiling heat transfer enhancement through surface modification," *International Journal of Heat and Mass Transfer,* vol. 181, p. 122020, 2021/12/01/ 2021, doi: https://doi.org/10.1016/j.ijheatmasstransfer.2021.122020.
[24] S. A. Khan, M. A. Atieh, and M. Koç, "Micro-Nano Scale Surface Coating for Nucleate Boiling Heat Transfer: A Critical Review," *Energies,* vol. 11, no. 11, p. 3189, 2018. [Online]. Available: https://www.mdpi.com/1996-1073/11/11/3189.
[25] D. E. Kim, D. I. Yu, D. W. Jerng, M. H. Kim, and H. S. Ahn, "Review of boiling heat transfer enhancement on micro/nanostructured surfaces," *Experimental Thermal and Fluid Science,* vol. 66, pp. 173-196, 2015/09/01/ 2015, doi: https://doi.org/10.1016/j.expthermflusci.2015.03.023.
[26] J.-F. Roques, "Falling film evaporation on a single tube and on a tube bundle," EPFL, 2004 2004.
[27] R. Enright, N. Miljkovic, N. Dou, Y. Nam, and E. N. Wang, "Condensation on Superhydrophobic Copper Oxide Nanostructures," (in en), *Journal of Heat Transfer,* vol. 135, no. 9, p. 091304, 2013-09-01 2013, doi: 10.1115/1.4024424.

[28] Y. Nam and Y. S. Ju, "A comparative study of the morphology and wetting characteristics of micro/nanostructured Cu surfaces for phase change heat transfer applications," *Journal of Adhesion Science and Technology,* vol. 27, no. 20, pp. 2163-2176, 2013/10/01 2013, doi: 10.1080/01694243.2012.697783.
[29] Y. Nam, S. Sharratt, G. Cha, and Y. S. Ju, "Characterization and Modeling of the Heat Transfer Performance of Nanostructured Cu Micropost Wicks," (in en), *Journal of Heat Transfer,* vol. 133, no. 10, p. 101502, 2011-10-01 2011, doi: 10.1115/1.4004168.
[30] K. Sahu, R. Singhal, and S. Mohapatra, "Morphology Controlled CuO Nanostructures for Efficient Catalytic Reduction of 4-Nitrophenol," (in en), *Catalysis Letters,* vol. 150, no. 2, pp. 471-481, 02/2020 2020, doi: 10.1007/s10562-019-03009-w.
[31] M. Liu, M. C. Lin, and C. Wang, "Enhancements of thermal conductivities with Cu, CuO, and carbon nanotube nanofluids and application of MWNT/water nanofluid on a water chiller system," *Nanoscale Research Letters,* vol. 6, no. 1, p. 297, 2011/04/05 2011, doi: 10.1186/1556-276X-6-297.
[32] M. Habert and J. R. Thome, "Falling-film evaporation on tube bundle with plain and enhanced tubes—Part I: Experimental results," *Experimental heat transfer,* vol. 23, no. 4, pp. 259–280, 2010 2010.
[33] B. S. Petukhov, "Heat Transfer and Friction in Turbulent Pipe Flow with Variable Physical Properties," in *Advances in Heat Transfer*, vol. 6: Elsevier, 1970, pp. 503-564.
[34] C. D. A. Inc. "Copper.org - C12200 Alloy." (accessed.
[35] P. F. Dunn, *Measurement, Data Analysis, and Sensor Fundamentals for Engineering and Science*, Boca Raton: CRC Press LLC, 2011.
[36] I. BIPM, I. IFCC, I. ISO, and O. IUPAP, "Evaluation of measurement data—guide to the expression of uncertainty in measurement, JCGM 100: 2008 GUM 1995 with minor corrections.," *Joint Committee for Guides in Metrology,* 2008.
[37] B. D. Bock, "Surface influences on falling film boiling and pool boiling of saturated refrigerants," (in en), p. 191, 2020 2020.
[38] W. Nusselt, "Die oberflachenkondensation des wasserdamphes," *VDI-Zs,* vol. 60, p. 541, 1916.
[39] M. G. Cooper, "Saturated nucleate pool boiling-a simple correlation," 1984 1984, pp. 785–793.
[40] V. H. Atlas, "VDI-Gesellschaft Verfahrenstechnik und Chemieingenieurwesen (GVC)," *Ch. Part D-Thermophysical Properties, ed: Springer-Verlag, Berlin/Heidelberg Germany,* pp. 121–613, 2010 2010.
[41] W.-T. Ji, C.-Y. Zhao, Y.-L. He, and W.-Q. Tao, "Experimental validation of Cooper correlation at higher heat flux," *International Journal of Heat and Mass Transfer,* vol. 90, pp. 1241–1243, 2015 2015.
[42] H. Li and P. Hrnjak, "Heat transfer coefficient, pressure drop, and flow patterns of R1234ze(E) evaporating in microchannel tube," (in en), *International Journal of Heat and Mass Transfer,* vol. 138, pp. 1368-1386, 08/2019 2019, doi: 10.1016/j.ijheatmasstransfer.2019.05.036.
[43] D. Gorenflo, E. Baumhögger, G. Herres, and S. Kotthoff, "Prediction methods for pool boiling heat transfer: A state-of-the-art review," (in en), *International Journal of Refrigeration,* vol. 43, pp. 203-226, 07/2014 2014, doi: 10.1016/j.ijrefrig.2013.12.012.
[44] U. Sajjad, I. Hussain, and C.-C. Wang, "A high-fidelity approach to correlate the nucleate pool boiling data of roughened surfaces," (in en), *International Journal of Multiphase Flow,* vol. 142, p. 103719, 09/2021 2021, doi: 10.1016/j.ijmultiphaseflow.2021.103719.
[45] J. F. Roques and J. R. Thome, "Falling films on arrays of horizontal tubes with R134a, part 1: Boiling heat transfer results for four types of tubes," *Heat Transfer Engineering,* vol. 28, no. 5, pp. 398-414, 2007.
[46] M. Christians and J. R. Thome, "Falling film evaporation on enhanced tubes, part 1: Experimental results for pool boiling, onset-of-dryout and falling film evaporation," *International Journal of Refrigeration,* vol. 35, no. 2, pp. 300-312, 2012.
[47] D. Jung, K. An, and J. Park, "Nucleate boiling heat transfer coefficients of HCFC22, HFC134a, HFC125, and HFC32 on various enhanced tubes," *International Journal of Refrigeration,* vol. 27, no. 2, pp. 202-206, 3// 2004, doi: http://dx.doi.org/10.1016/S0140-7007(03)00124-5.
[48] Y. Lee, D.-G. Kang, J.-H. Kim, and D. Jung, "Nucleate boiling heat transfer coefficients of hfo1234yf on various enhanced surfaces," *International Journal of Refrigeration,* vol. 38, pp. 198-205, 2014, doi: http://dx.doi.org/10.1016/j.ijrefrig.2013.09.014.
[49] M. Cooper, "Saturation nucleate pool boiling: A simple correlation," in *Institute of Chemical Engineering Symposium Series*, 1984, vol. 86, no. 2, 1984, pp. 785-793.
[50] W.-W. AG", "Wieland GEWA-K, GEWA-KS - Low-finned Tubes." [Online]. Available: https://www.wieland.com/en/Media/Files/brochures/wieland-gewa-k-gewa-ks-low-finned-tubes.pdf